Journal of Structural Geology 31 (2009) 194–207

Contents lists available at ScienceDirect

Journal of Structural Geology

journal homepage: www.elsevier.com/locate/jsg

Faulting and deformation in chalk

P. Gaviglio [a,b,*], S. Bekri [c], S. Vandycke [d], P.M. Adler [e], C. Schroeder [f,h], F. Bergerat [g], A. Darquennes [h], M. Coulon [i]

[a] EA 2642 Géosciences, Université de Franche-Comté, 16 Route de Gray, 25030 Besançon cedex, France
[b] IUFM, Fort Griffon, 25042 Besançon cedex, France
[c] Institut Français du Pétrole, 1 et 4, avenue du Bois-Préau, 92852 Rueil-Malmaison cedex, France
[d] FNRS, Faculté Polytechnique de Mons, Géologie Fondamentale et Appliquée, 9 rue de Houdain, 7000 Mons, Belgique
[e] Sisyphe, UMR 7619 CNRS, Université Pierre et Marie Curie, case 123, 4 place Jussieu, 75252 Paris, France
[f] UCL, Dépt Génie Civil & Environnement, 1459 Louvain-La-Neuve, Belgique
[g] Laboratoire de Tectonique, UMR 7072 CNRS Université Pierre et Marie Curie, case 117, 4 place Jussieu, 75252 Paris, France
[h] Service BATir Université Libre de Bruxelles 50, av. Roosevelt, 1050 Bruxelles, Belgique
[i] Laboratoire des Sciences de la Terre, CRA, 2, esplanade Roland Garros, 51100 Reims, France

ARTICLE INFO

Article history:
Received 15 March 2007
Received in revised form
25 October 2008
Accepted 20 November 2008
Available online 7 December 2008

Keywords:
Chalk
Normal faulting
Reconstructed porous media
Shear deformation band
Permeability
Deformation models

ABSTRACT

In chalk, strong deformation at the grain level is associated with faulting. Within a 5–10 cm thick fringe on each side of normal faults, texture modifications were documented and analysed in samples from the Campanian White Chalk. We used SEM observations, image analysis, reconstruction of the porous media and physical measurements. Dissolution and cementation features, together with a reorganisation of the pore space, can be explained by massive fluid transfers. Faulting is interpreted as ductile shearing, which involves slip and dissolution first in shear deformation bands and then along a single fault plane.

1. Introduction

During fault propagation in the brittle field, deformation is distributed along several discontinuities. Generally in the first steps, en échelon arrays of tension cracks and shear fractures, are formed; depending on the mechanical conditions and heterogeneities (lithology, cementation, thickness variations), various associations of fractures may develop and produce different patterns, with transpression and transtension zones with consistent orientations (Hancock, 1972; Segall and Pollard, 1980; Gamond, 1983). When the slip surfaces are able to link to one another, creating more or less lens shaped blocks (Tchalenko, 1970), the displacements increase and the faulted zones become wider. Displacements beside the main fault are distributed over an increasing number of structures (Shipton and Cowie, 2001; Du Bernard et al., 2002). These structures are either sharp discontinuities or deformation bands (Aydin et al., 2006). In deformation bands the texture of the parent rock is modified. Translation and rotation, fracturing of grains and dissolution are the main modes of deformation at the grain scale. The change in texture commonly produces a change in porosity (e.g. Aydin et al., 2006).

At low confining pressure, little or no cataclasis is involved and porosity increases, dilatancy occurs. At high confining pressure, compaction and cataclasis produce a decrease in porosity (Antonellini et al., 1994; El Bied et al., 2002) but the experimental approach shows that dilatancy is produced on each side of the compacted slip bands (El Bied et al., 2002). In limestones, fault zones are common and cataclasis seems to be the predominant phenomenon along the shear fractures, especially in well-cemented rocks. However, dissolution and precipitation are commonly associated, and stylolites and tension gashes are common features (Hancock, 1985).

* Corresponding author. IUFM de Franche Comte, Fort Griffon, 25042 Besancon, France. Tel.: +33 3 81 65 71 82; fax: +33 3 81 82 02 55.
E-mail addresses: patrick.gaviglio@fcomte.iufm.fr (P. Gaviglio), samir.bekri@ifp.fr (S. Bekri), sara.vandycke@fpms.ac.be (S. Vandycke), pierre.adler@upmc.fr (P.M. Adler), christian.schroeder@ulg.ac.be (C. Schroeder), francoise.bergerat@upmc.fr (F. Bergerat), adarque@ulb.ac.be (A. Darquennes), michel.coulon@univ-reims.fr (M. Coulon).

0191-8141/$ – see front matter © 2008 Elsevier Ltd. All rights reserved.
doi:10.1016/j.jsg.2008.11.011

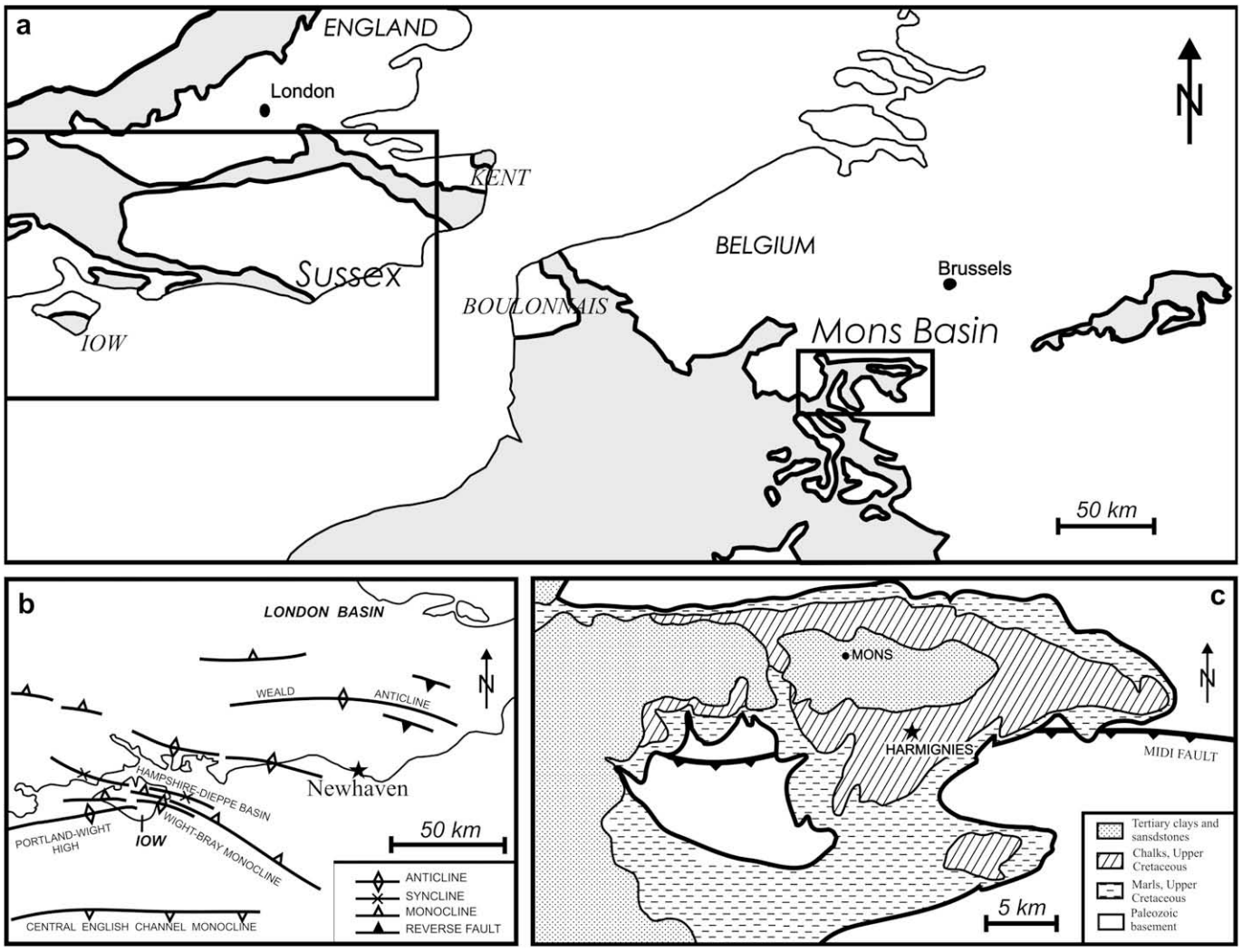

Fig. 1. Regional setting. (a) Location of the chalk basin (grey areas) in northwestern Europe. (b) Sussex. (c) Mons basin. IOW: Isle of Wight; stars: locations of the investigated sites (Newhaven and Harmignies).

Tondi et al. (2006) reported three major processes involved in faulting of grainstones: strain localisation (forming compaction bands), pressure solution and shearing of stylolites. When pressure solution occurs inside the compaction bands, it induces shearing and massive cataclasis with stylolites. Tondi (2007) emphasises the effect of the pressure solution overprinting earlier compactive shear bands.

Fluid circulation is a major factor in faulting; crystallisation features at any scale are evidence of the close relation between block displacements and fluid migrations. Fault-related permeability is obviously a predominant factor in rock deformations. Caine et al. (1996) reported that the fault core (where cataclasis and anastomosed slip surfaces are predominant) and the damage zone (formed by related microfaults and tension gashes) form contrasted media. The permeability in the fault core is bound to be lower than in the damage zone. The actual behaviour of the fault depends on geometry, thickness and connection of the two zones. In any case, a fault or a fault zone is a discontinuity that may modify fluid circulations. It may be a conduit or a barrier, or behave as a combined barrier–conduit system.

Chalk is a homogeneous material in which macroscopic and microscopic observations do not allow detection of major modifications as they do in sandstones or even carbonate grainstones. Diagenetic and tectonic strains in chalk can be detected and quantified using SEM observations or physical measurements (Mimran, 1975; Mimran and Michaeli, 1986; Jones and Leddra, 1989; Matthews et al., 1996; Borre and Lind, 1996). The mechanical behaviour of chalk is multimechanism stress dependent, with a strong hydro-mechanical coupling: it exhibits elasto-brittle behaviour at low to mean stress levels. At high stress levels the chalk follows an elastoplastic constitutive law with pore collapse followed by hardening (Schroeder, 2003). Field observations and measurements of physical characteristics carried out on White Chalk from the Mons Basin have shown evidence of significant horizontal shortening by dissolution against fault planes (Gaviglio et al., 1999; Angelier et al., 2006); the matrix strains detected are concentrated in 50 mm thick bands bordering the fault planes on either side. By studying this material our purpose was to try to understand the interactions at the grain scale between the fault plane and the calcite matrix and to propose a model for this atypical faulting process. Faults having undergone only one brittle deformation phase were selected.

2. Investigated sites

Two sites with well known normal faulting were selected in the Campanian White Chalk (Fig. 1). In both cases this chalk is a very pure material with a porosity close to 40%:

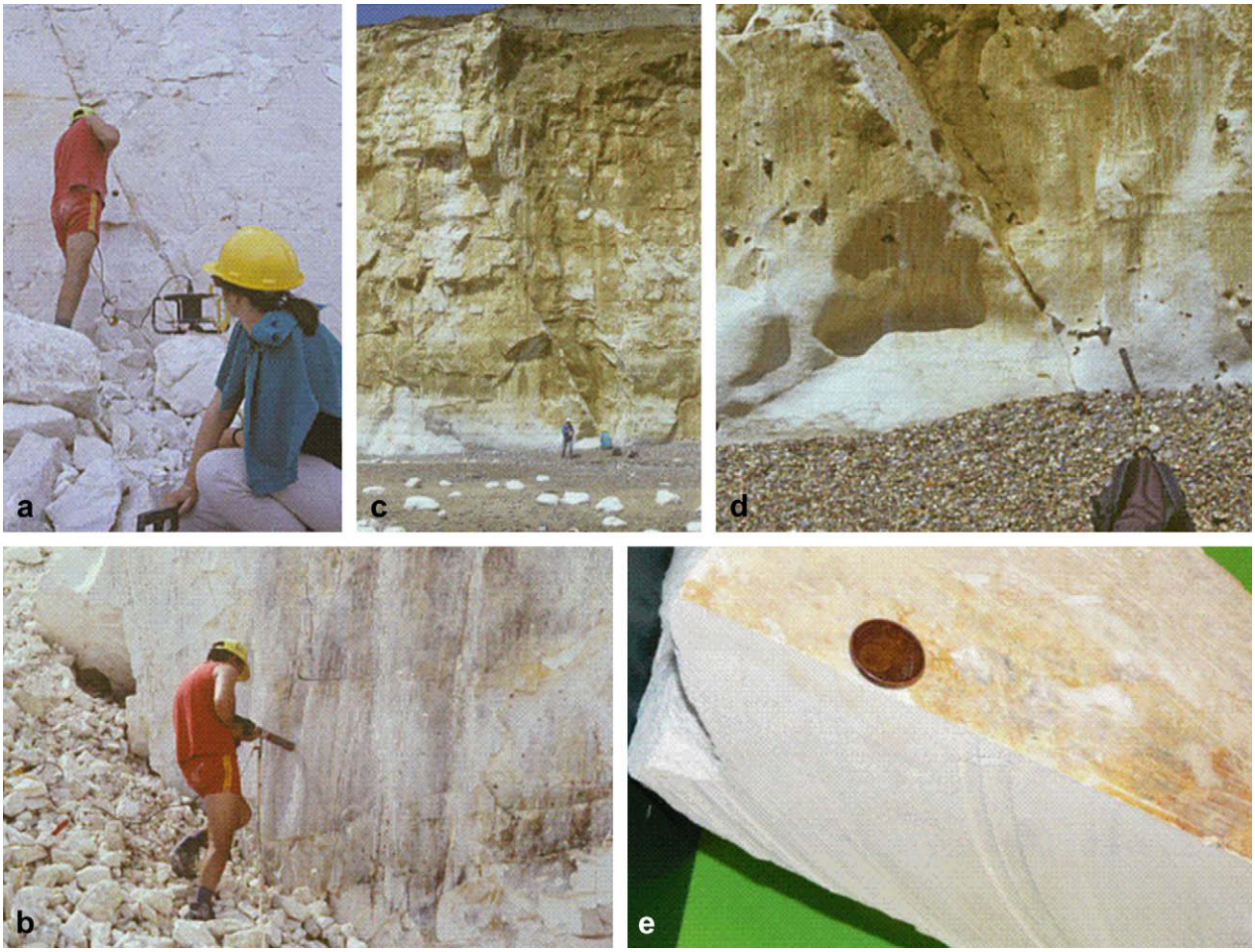

Fig. 2. Views of the fault planes. (a) Fault plane in the Harmignies quarry. The fault plane is roughly perpendicular to the quarry face. (b) Close-up view of a fault plane in the same quarry. (c) Normal faults in the Newhaven cliff. (d) Close-up view of the Newhaven sampling site. (e) Block showing striations on a fault plane in White Chalk. To the naked eye the chalk close to the contact seems to be unaffected by deformation.

- Harmignies, in the Mons Basin (Belgium), in a quarry belonging to CBR (Ciments Belges Réunis). Two faults, 200 m apart, were studied: one created during the Maastrichtian NE–SW extension, the other during the Upper Campanian NW–SE extension. Former studies are based on samples and data from this site (Vandycke and Bergerat, 1989; Vandycke et al., 1991; Vandycke, 1992; Gaviglio et al., 1993, 1997).
- Newhaven in Sussex (United Kingdom): sampling was carried out on the coastal cliff.

The studied fault belongs to a system postdating the Eocene inversion phase (Vandycke, 2002). It may correspond to the extensional episode that prevailed in Western Europe during the Oligocene. The chalk contains flint beds.

Table 1
Fault planes and associated profiles.

Site	Fault plane and striation orientation	Downthrow of the fault (m)	Name of profile
Newhaven	N160 75E 58S	0.55	Newhaven
Harmignies	N131 85 N 80E	1.00	Mons I.1
Harmignies	N131 85 N 80E	1.00	Mons I.2
Harmignies	N055 67S 82 N	1.70	Mons VI.2

The fault planes are sharp discontinuities according to classification by Aydin et al. (2006). They are flat, gently striated, with no tension or shear fractures associated, and the rock is not brecciated (Fig. 2b,c and e). The rock matrix is homogeneous and looks similar to the intact parent rock (Fig. 2e). The break up pattern (Fig. 2b,c and d) is the consequence of jointing, either natural or artificial (due to quarry exploitation). Brittle deformation is localised along a single plane. Furthermore, no evidence of fault drag deformation could be found either in the footwall or in the hangingwall. Therefore, the blocks of chalk can be assumed to have remained rigid throughout the activity of the faults. No particular macroscopic features were observed on the samples except at Newhaven, where some cracks, a few millimetres long, about 0.5 thick and filled with calcite, exist in a 10–15 mm wide fringe along the fault plane.

The effect of dissolution was estimated by 2D and 3D analytical models of along-fault belemnite rotation quantified in the field (Angelier et al., 2006), which accounts for a minimum 50 mm horizontal shortening, and for about 1 m in vertical displacement of the fault. Laboratory measurements (mercury porosimetry, capillary rise, elastic waves velocity) allowed us to assess the changes in porosity along faults (Schroeder et al., 2006). If the drop in porosity occurred in a closed system, the horizontal shortening can be estimated from 1 to 10 mm. This is a minimum value: an open system assumption would give higher results (Gaviglio et al., 1999).

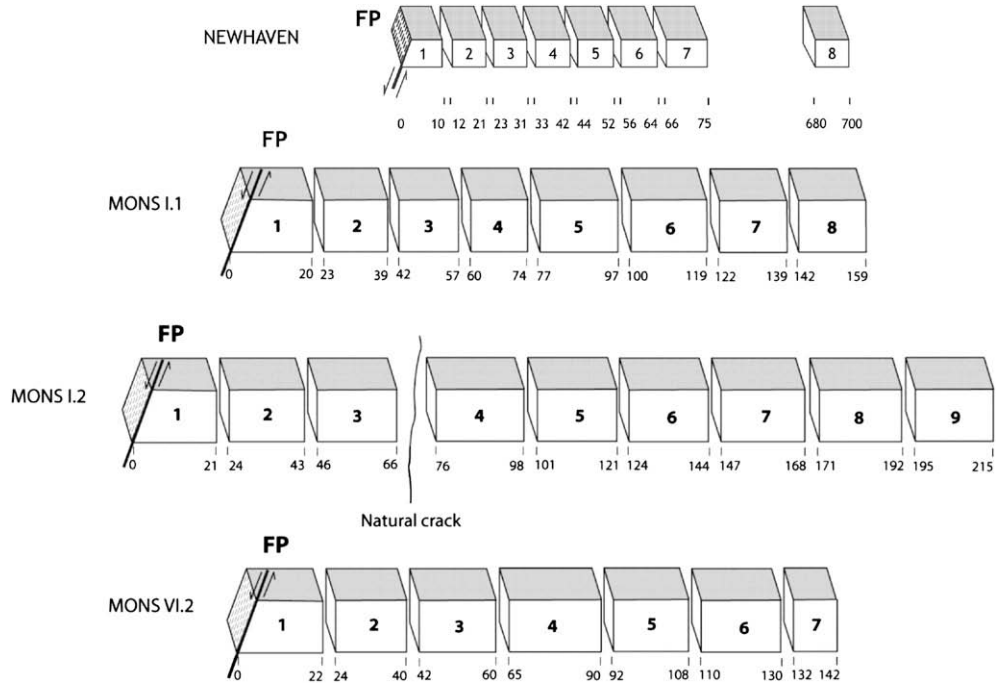

Fig. 3. Display of the plugs of chalk obtained for each profile and their distance to the fault planes (mm).

The validity of the open system assumption, more plausible in this medium, is demonstrated by the minimum estimate of 50 mm horizontal shortening from the belemnite rotation. A consequence is that a roughly 50 mm thick band of chalk is missing along fault planes with a 1 m downthrow.

3. Method and techniques

3.1. Sampling and preparation of the plugs

In Newhaven (Fig. 2c and d), one block was extracted against the fault and another one, for reference, was taken at 70 cm. In Harmignies (Fig. 2a and b), coring was carried out on two outcropping fault planes (Mons I.1 and Mons I.2 on the same plane). All samples were taken along the bedding which is nearly horizontal in both cases. The recovered samples and the associated profiles are listed in Table 1.

The samples were cut into plugs (Fig. 3). The upper part of the plugs, which coincides with the bedding, was selected for SEM observations. Plugs along a parallel profile, or located just below the first set, were prepared for physical measurements. The plugs to be used for SEM observations were impregnated with resin by capillary rise in order to strengthen the rock without modifying its grain-scale structure. The consolidated plugs were sawed and the saw cut was gently polished.

3.2. Collection of SEM data

Observations were made at regularly distributed points (four or five per plug). In order to assess more accurately the porosity changes over short distances, where strains are maximum, more data were gathered between 0 and 20 mm from the fault planes (14 or 16 points). Most of the survey consisted in obtaining digital data directly. The back-scattered electron mode was used. The images display 256 grey-levels; calcite and voids are respectively bright and dark. For plugs from Newhaven and Mons I.2, magnifications of 50 and 2000 were used to explore porosities from the same spots on both the 0.1 millimetre scale and the micrometre scale. Those from Mons I.1 were analysed with a magnification of 350 only so as to allow to record the whole range of pore sizes. However, the smallest voids cannot be detected and many big voids formed by fossils are recorded. Moreover, small differences in microporosity may be amplified during the erosion–dilatation processing of the images. Obviously a magnification of 2000 is much more reliable. The captured images, with magnifications of 50, 350 and 2000, are listed in Table 2.

3.3. Image analysis

Image analysis was performed in two different ways: (i) a qualitative observation of the digital images to detect significant features such as aggregated grains or cemented areas; (ii) a quantitative analysis, using Visilog software®.

The digital images underwent the usual processing necessary for binary images, namely determining a threshold and applying dilatation and erosion. Processing was based on three principles: (i) finding porosity by area measurement close to the values obtained by mercury injection on an adjacent plug; (ii) abiding, as much as possible, by the shapes shown by the digital images; (iii) using the same processing for all digital images in a given series (same profile, same magnification).

Table 2
Captured digital images.

	Newhaven	Mons I.1	Mons I.2	Mons VI.2
Plugs number	8	8	9	7
×50 images number	36		17	
×350 images number		44		
×2000 images number	36		54	121
Total images number	72	44	71	121
Investigated length (mm)	80	160	215	146
Reference sample	700 mm			
Reconstructed media	11	12	10	11

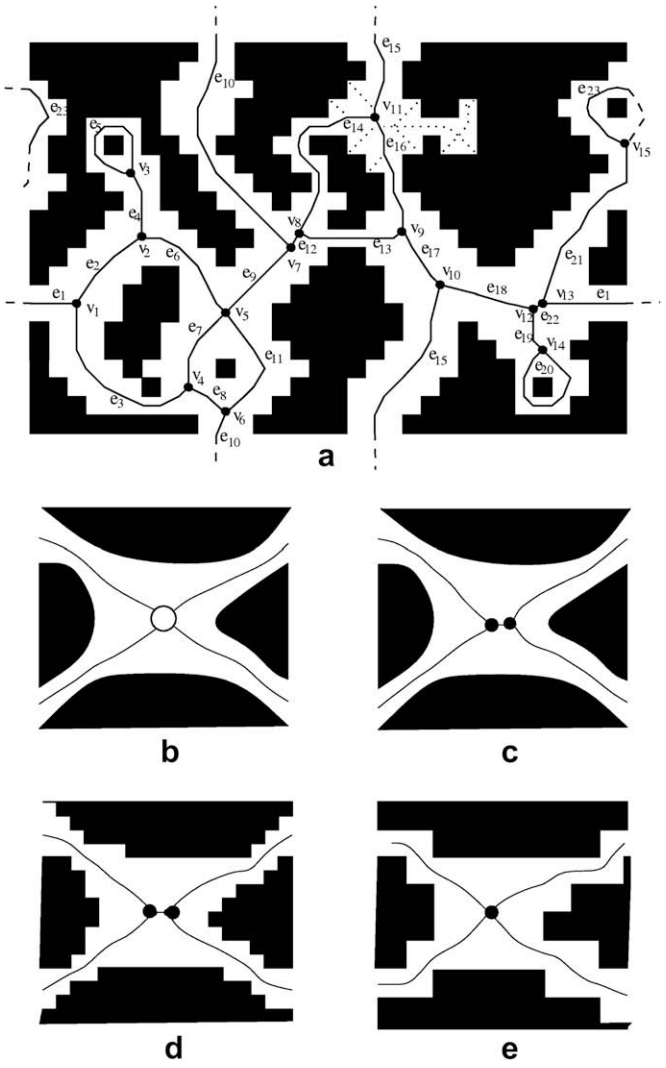

Fig. 4. Characteristics of the pore space skeleton in a 2D spatially periodic medium (a) (Thovert et al., 1993). The edges are labelled e_i ($i = 1, \ldots, 23$), and the vertices v_j ($j = 1, \ldots, 15$). The cyclomatic number is $\beta_1 = 9$. The continuations of edges by periodicity across the cell boundaries are indicated by broken lines. The dotted lines around v_{11} are examples of dead-ends, which are primed during computation. A local situation is detailed in (b–e). It is similar to the cavities around the vertices (v_7, v_8) or (v_{12}, v_{13}). The geometry is given in (b), together with an intuitive pore/throat representation (one pore with $z = 4$ throats). The exact skeleton is sketched in (c), with two vertices separated by a short edge. Two possible numerical determinations are given in (d, e) with different resolutions which yield one or two vertices in the cavity. The cyclomatic number is the same in all cases (b–e).

The statistical geometrical characteristics of the pore space (porosity and correlation length) were measured for each captured binary image (Adler et al., 1990, 1992). An average value, derived from the individual images analysis, was calculated for each plug. These data were used to draw the porosity curves (porosity referred to as SEMε).

3.4. Reconstruction of the porous media

Various measurements are performed on the digitised images of the plug sections of chalk. Each section is described by a $L_x \times L_y$ matrix of square binary pixels which take the values 0 or 1 in the solid or pore phases, respectively. The physical dimension of these pixels is denoted by p. The phase function $Z(\mathbf{x})$ is defined as

$$Z(\mathbf{x}) = \begin{array}{ll} 1 & \text{if } \mathbf{x} \text{ belongs to the pore space} \\ 0 & \text{otherwise} \end{array} \quad (1)$$

where $\mathbf{x}$ denotes the position with respect to an arbitrary origin.

The porosity ε and the correlation $R_z(\mathbf{u})$ can be defined by the statistical average given in brackets $\langle\ \rangle$.

$$\varepsilon = \langle Z(\mathbf{x}) \rangle$$

$$R_z(\mathbf{u}) = \frac{\langle (Z(x) - \varepsilon)(Z(x+u)) - \varepsilon \rangle}{\varepsilon(1-\varepsilon)} \quad (2)$$

For isotropic materials, $R_z(\mathbf{u})$ is a function of the modulus of the lag $u = \|\mathbf{u}\|$ only, and $R_z(\mathbf{u}) = R_z(u)$. Otherwise, the correlations for $\mathbf{u}$ parallel to the x- and y-axes are denoted by R_{Zx} and R_{Zy}, respectively.

These two quantities are measured for each section by image analysis. The porosity is obtained by averaging. The correlation function (2) was evaluated for each section by using standard translation and intersection routines. The increment u is varied pixel by pixel. The correlation length L is defined as the integral of the correlation function

$$L = \int_0^\infty R_Z(u)\mathrm{d}u \quad (3)$$

For anisotropic materials, L_x and L_y are derived accordingly from R_{Zx} and R_{Zy}.

We now briefly sketch the reconstruction of three-dimensional random media which is fully described in Adler et al. (1990). We want to generate a three-dimensional random porous medium with a given porosity ε and a given correlation function; the medium is homogeneous and isotropic, but this last property is not essential.

This is equivalent to generating a random function of space $Z(\mathbf{x})$ which is equal to 0 in the solid phase and to 1 in the pore phase. $Z(\mathbf{x})$ has to verify the two average properties in equation (2). For practical purposes only, the porous medium is constructed in a discrete manner. It is considered to be composed of N_c^3 small cubes, each of the same size a. These elementary cubes are filled either with void or with solid. Moreover, because of the spatial periodicity, all the physical quantities are independent of the choice of the origin and of the faces of unit cells. Details of the algorithm can be found in Adler (1992) and Adler and Thovert (1998).

Once the porous medium has been generated, its geometry and its topology can be characterised. First, the skeleton of the pore space is determined; it can be viewed as a simplified image of the pore space, analogous to a capillary network (Fig. 4). It is determined by a progressive conditional thinning algorithm (Thovert et al., 1993). The cyclomatic number β is equal to

$$\beta = m - n + 1 \quad (4)$$

where m and n are the number of edges and vertices in the graph, respectively. For a statistically homogeneous medium, it is more appropriate to introduce the volumetric numbers of cycles per cubic micrometre and per volume L^3, respectively.

Various statistical quantities can be measured on the skeleton and are illustrated in Fig. 3. Let d_s denote the distance of a point on the skeleton to the closest solid. Its minimum r_e along the edge e is the critical radius of this edge, i.e., the radius of the largest sphere which can travel along e. d_e is the end-points distance of an edge, i.e., the distance between the two vertices located at the end of the edge. r_v is the vertex radius defined as the radius of the largest sphere centred at the vertex which fits inside the pore space. The coordination number z_v is the number of edges of a given vertex.

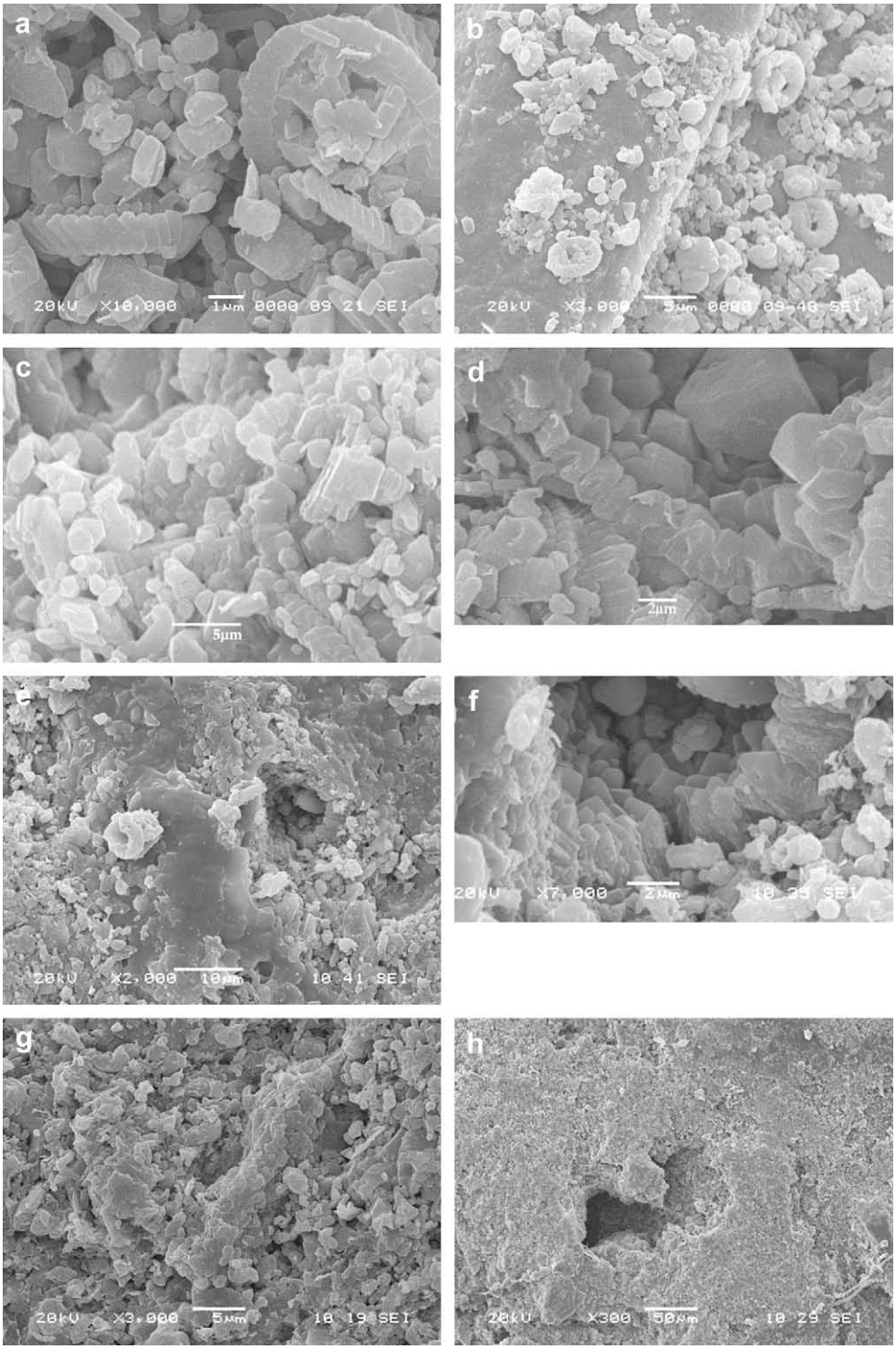

Fig. 5. SEM photographs (White Chalk from Harmignies). (a) Intact parent rock made up of coccoliths and platelets, with a porosity of about 40%. (b) Fault plane formed by a continuous coating of calcite; the linear feature is a striation. (c) Compact area formed by tightly packed platelets. (d) Small indentations indicating dissolution at grain to grain contacts. (e) Cemented platelets due to calcite deposition forming a wall-like structure. (f) neoformed calcite crystals. (g) A large aggregate formed by platelets cemented together by calcite overgrowths. (h) A large pore opening on a fault plane surface.

Statistics relative to the elements of the skeleton may prove useful to feed a capillary network model of the porous material. Averages, standard deviations and histograms of r_e, d_e, r_v and z_v can be systematically evaluated.

The quantities introduced in the previous paragraph are measured on the mathematical skeleton (points at the largest possible distance from the solid, i.e., points at equal distances from several solid walls), which may differ quite significantly from an intuitive pore/throat vision of the pore space.

Forty-four images were selected for generating reconstructed media with the same porosity and the same correlation function as the real media. This reconstruction was used for calculating the

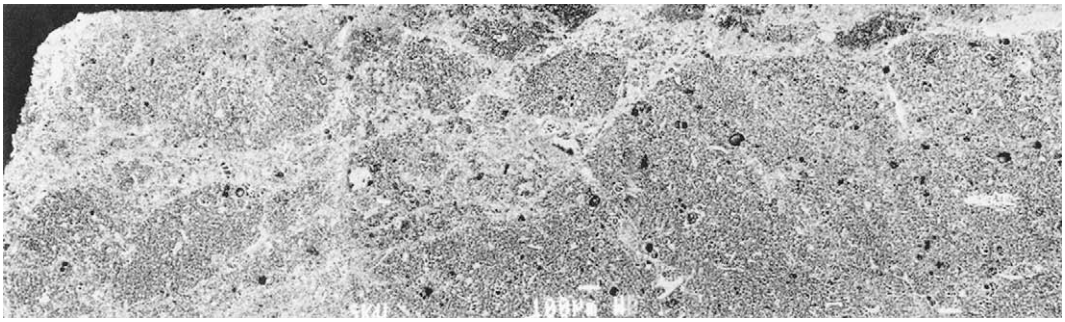

Fig. 6. SEM photograph of a 1.5 mm wide fringe bounding a fault plane. The walls are more compact bands (the clearest areas). They are a consequence of cementation. The darkest patches, nearly circular in shape, are voids of foraminifera shells. The fault plane corresponds to the upper limit of the figure.

permeability and conductivity tensors. The latter may be used for determining the diffusion properties. A geometrical analysis of the reconstructed media was used in order to provide information on the spatial organisation and dimensions of the porous medium in chalk, namely pore radii, "tube" radii and lengths, coordination of pores. It was carried out on images of profile Mons I.2.

3.5. Physical measurements

Porosity measurements by mercury injection or by saturation with water are referred to as Hgε and Wε respectively (ε: porosity value). Besides the pore volume of the material, the pore access radii can be obtained by mercury injection. These radii are directly comparable with the edge radii determined through the above-mentioned reconstruction. The measurements were performed on samples with a volume ranging from 1 cm^3 (mercury injection) to 5 cm^3 (water saturation).

Some permeability measurements were carried out for comparison with the values obtained by the reconstructed media method. They were performed using a Ruska Liquid Permeameter with a constant head. Water was injected into cylindrical plugs ($D = 10$ mm, $L = 20$ mm) with a pressure of 0.1 MPa, applied by compressed air.

Table 3
Qualitative observations collected along the four profiles.

Newhaven	Plug 1	2	3	4	5	6	7	REF	
Compact matrix	×		×					×	
Aggregates	×	×	×	×					
Large size aggregates	×	×				×			
Crystallines shapes	×	×	×	×			×		
Walls	×								
Indentations		×							
Large pores	×	×	×	×		×			
Heterogeneous packing	×	×	×						
MONS I.1	Plug 1	2	3	4	5	6	7	8	
Compact matrix	×	×							
Aggregates	×	×		×					
Large size aggregates	×								
Crystallines shapes	×								
Walls	×								
Indentations									
Large pores	×					×			
Heterogeneous packing	×								
MONS I.2	Plug 1	2	3	4	5	6	7	8	9
Compact matrix	×							×	
Aggregates	×	×	×	×	×	×	×	×	
Large size aggregates	×	×	×	×				×	
Crystallines shapes	×			×					×
Walls	×				×		×	×	×
Indentations	×								
Large pores		×	×		×				×
Heterogeneous packing	×	×	×				×		×
MONS VI.2	Plug 1	2	3	4	5	6	7		
Compact matrix	×	×							
Aggregates	×	×	×						
Large size aggregates									
Crystallines shapes	×	×	×	×					
Walls									
Indentations				×	×				
Large pores	×								
Heterogeneous packing	×	×	×	×					

4. Results

4.1. General remarks

Chalk is made up of calcite particles, mainly platelets from broken up coccoliths, whole coccoliths and rare coccospheres. The length of the platelet edges ranges between 0.5 and 2 μm; most of the interstitial voids forming the pores are on the same scale (Fig. 5a). This porosity, which is referred to as microporosity in this paper, is clearly observable with a magnification of 2000. The pores formed by the cells of foraminifera, the biggest voids observable in chalk matrix, range between 20 and 100 μm. They are referred to as mesopores and can be observed with a magnification of 50 without being confused with micropores.

4.2. Qualitative observations

The role of the three following processes, compaction, calcite deposition and dissolution can be inferred from various observations of the textures. The textural features are described and illustrations are given (Fig. 5) with respect to each process.

i Compaction: Compact arrangement with a condensed matrix where the coccolith platelets are more tightly packed than in the intact parent rock (Fig. 5c); in this arrangement indentations between adjacent particles can be observed.

ii Calcite deposition:
- calcite overgrowths on coccolith platelets or neoformed isolated calcite crystals (Fig. 5f);
- calcite cement making bridges between the particles producing aggregates in which the original particles are more or less discernible (Fig. 5e);
- large aggregates exceeding 10 μm (Fig. 5g);
- walls: observed in Mons chalk at low magnification (Fig. 6). Some samples display a few narrow wall-like calcite discontinuities, more or less parallel to the fault plane. Detailed observations with a higher magnification show

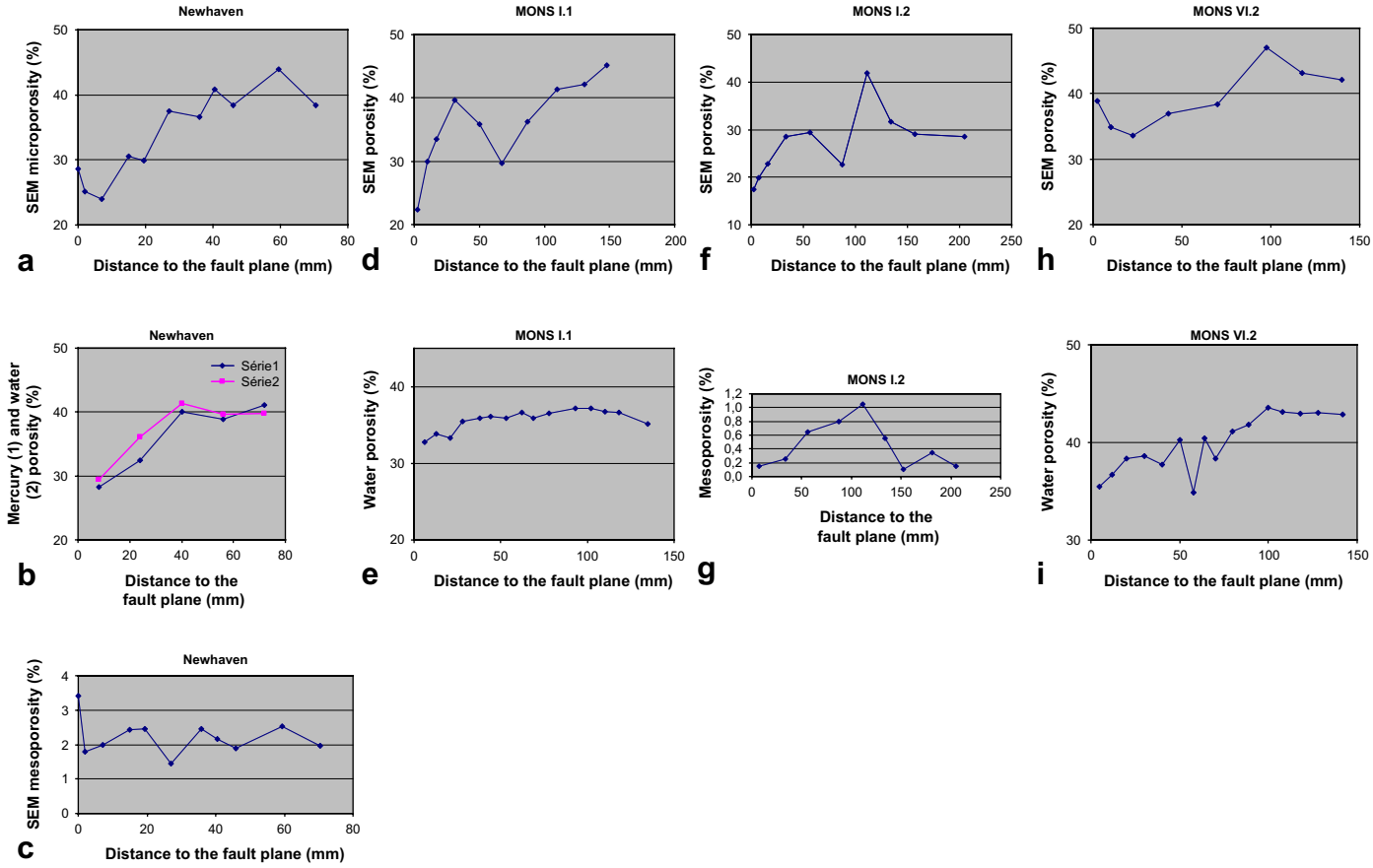

Fig. 7. Porosity profiles based on SEMε (a, c, d, f–h), Wε (b, e and i), Hgε (b). All SEMε profiles display the variations in microporosity (magnification of 2000 or 350) except profiles c and g (mesoporosity observed with magnification of 50).

that they are not real cracks, but crystallisation zones with an increased density in calcite crystals, with no sharp boundaries, formed by concentrated cementation in the pore system (Fig. 5e). They have been observed in other faulted samples from the same quarry (Schroeder et al., 2006; Darquennes et al., 2006).

iii Dissolution
* indentation marks due to grain to grain contacts (Fig. 5d);
* large pores: formed in the matrix, not connected with foraminifera or other microfossils, with a diameter exceeding greatly the size of the original particles and of the interstitial voids; these pores, which look like channels, were interpreted as being the result of dissolution of pre-existing spaces (Fig. 5h).

Another feature derived from microscopic observations is the heterogeneous packing which is typical of materials with loose and compact arrangements closely juxtaposed. It is regarded as a consequence of the disruption of the initial packing. Qualitative observations are summarised in Table 3. Plugs limited on one side by the fault planes, display all the features of a modified matrix.

4.3. Porosity estimation and porosity profiles

In all samples a decrease in porosity occurs close to the fault planes (Fig. 7).

* Newhaven (Fig. 7a and b): the average values obtained by image analysis (SEMε) are in good agreement with the physical measurements (Hgε and Wε). Against the fault plane, porosity drops to 25–30%, where small cracks filled with calcite were observed. The mesoporosity, mainly due to microfossils, ranges between 1.4 and 3.4% (Fig. 7c). Some higher values against the fault plane may be ascribed to big pores in connection with the fault plane. Obviously the transformation of the porous medium essentially concerns the micropores. Access diameters, obtained from the mercury injection curves, are significantly lower in strained rock since they may drop from 0.6–0.7 μm to 0.4 μm.
* Mons I.1 – While SEMε values (Fig. 7d), vary from 45 to 22%, physical measurements (Wε, Fig. 7e) indicate a much smaller variation. This difference may be ascribed to the influence of magnification of 350 (see Section 3.2). Two measurements by mercury injection, in unstrained material yielded 38.2 and 38.6%.
* Mons I.2: The SEMε profile (Fig. 7f) is irregular, with a very low porosity zone. The reference values (Hgε) are 37.8 and 38.5% outside the profile. Mesoporosity does not exceed 1.1% (Fig. 7g). No water porosity was measured on this profile.
* Mons VI.2: SEMε and Wε profiles are comparable (Fig. 7h and i) but the data differ below 20 mm. The high values obtained through microscopic analysis against the fault plane can be accounted for by the local concentrations of large pores described above.

4.4. Reconstructed media

The properties of the reconstructed medium of one image are summarised in Fig. 8. Among these properties, special attention was paid to the pore radii, the pore access radii, the length of the "tubes" or the end-point distance and the coordination number.

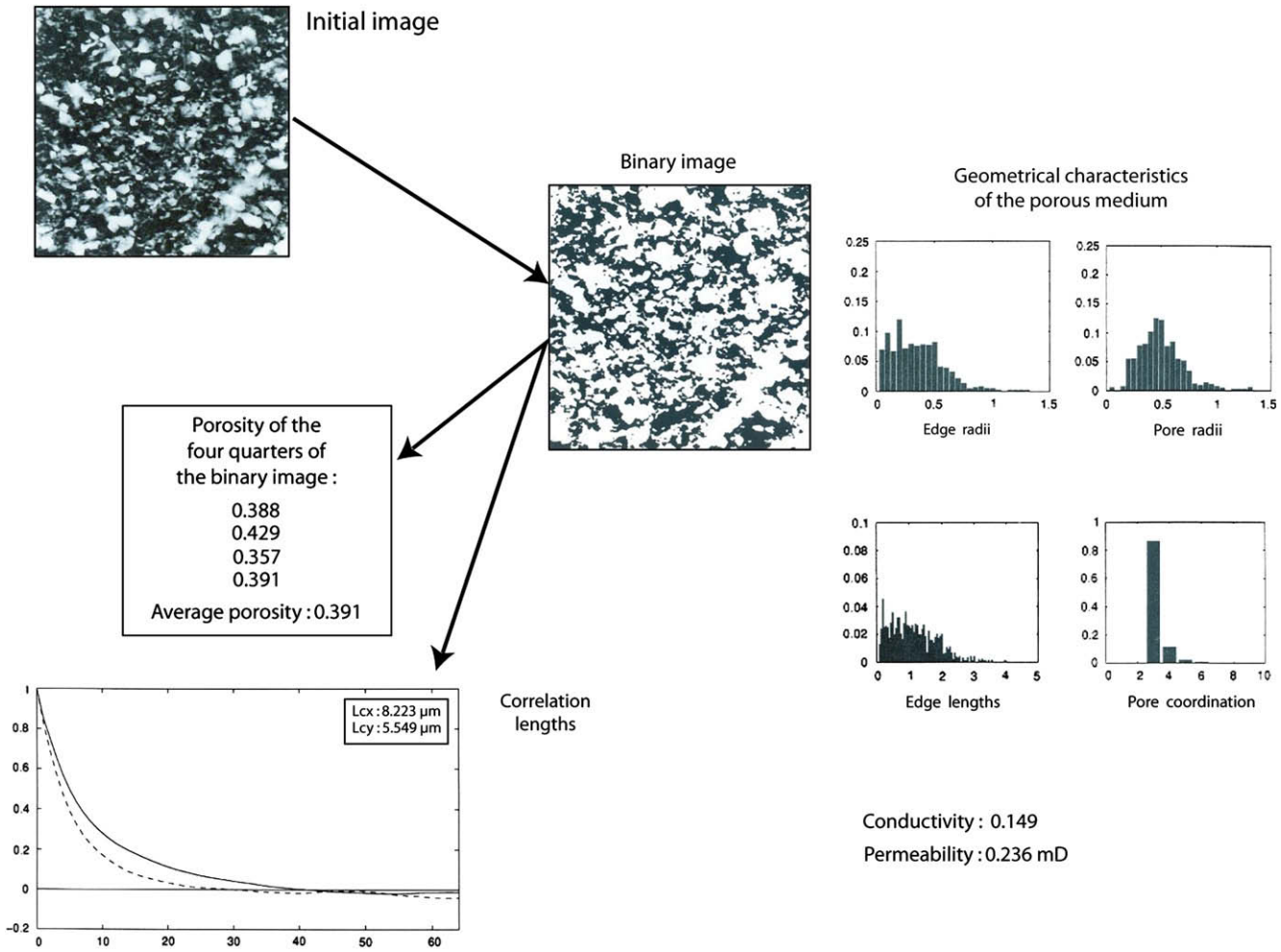

Fig. 8. Image properties. Example of a binary image obtained from a SEM photograph. The statistical characteristics of the binary image are used for generating the reconstructed medium. The properties of the reconstructed medium are used for calculating the permeability and the conductivity (see Section 3.4). The geometrical characteristics are yielded by image analysis (see Section 3.3).

Along the Mons I.2 profile (Fig. 9), porosity is reduced by a factor of 2 near the fault plane. The pore radii tend to decrease towards the fault plane (the mode decreases from 0.5 to 0.25 µm). The pore access radii and the end-point distance follow the same trend, and their size distribution becomes more regular. The same trend was detected by mercury injection for the pore access radii. Two characteristics were stable, namely the length of tubes around 1 µm, and the coordination of pores (3).

Calculated permeabilities, based on the micropore size distribution only, are smaller against the fault plane (Table 4). Values from the VI.2 sample were obtained from the 10 mm fringe only in order to compare the compact matrix permeability (K2) and the large pore matrix permeability (K3) from images where large pores could be observed. Values from Mons I.1 are not to be compared strictly with the other sets because the magnification used was not the same. The porosity for the Mons I.2 sample is divided by roughly 2. According to the model, the decrease in permeability is due partly to the reduction in pore size (factor 4) and partly to the reduction in porosity.

The calculated permeabilities are not in very good agreement with the laboratory measurements carried out on reference samples (between 2 and 3 mD for Newhaven and 0.2 and 1.5 mD for Mons). The calculations are based on micropores only and do not take into account the mesopores. The elementary representative volumes are significantly different.

5. Interpretation

Fig. 10 is a schematic representation of the zoning, based on observations and measurements, of a 150 mm thick band parallel to a fault plane. This band is not a deformation band as described by Aydin et al. (2006). It forms a progressive transition between a fault plane, where transformation of the chalk is maximum, and the intact parent rock. Its most significant part is only 50 mm thick; the main matrix properties constraining the interpretation are displayed in Figs. 11 and 12. Three aspects have to be considered successively: the pore system pattern, fluid circulations and fracturing.

5.1. Pore system pattern

Microscopic observations and image analysis suggest that no discontinuous evolution exists in the material (Fig. 7a,d,f and h). The matrix changes are progressive, as shown by the measurements of porosity and pore access radii (Figs. 7b,e,i and 9), and seem to be controlled only by the distance to the fault plane. The void system does not display any internal organisation connected with fractures or cracks. Image analysis and reconstruction of the medium based on binary images from three perpendicular planes did not provide any evidence of preferential orientation of pores, or of the calcite grains. There is no observable evidence of cataclasis.

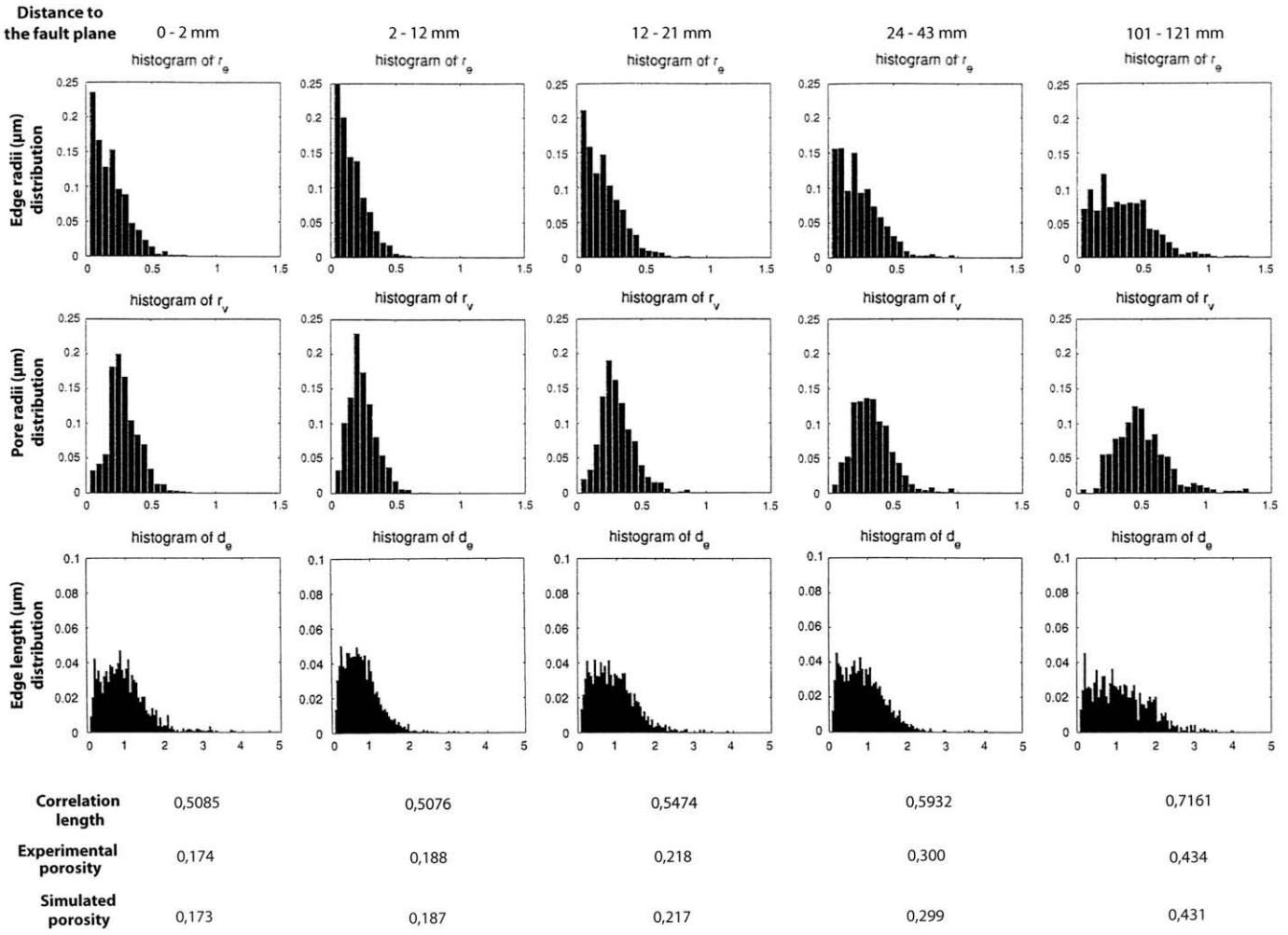

Fig. 9. Three profiles based on geometrical characteristics obtained through image analysis (Mons I.2). The edge radii and pore radii distributions are significantly modified close to the fault plane.

The cemented walls are the only anisotropic features (Schroeder et al., 2006; Darquennes et al., 2006): most of the large pores, which are the only observable connections between the unstrained chalk matrix and the fault planes, are found in these structures (Figs. 5g and 12).

5.2. Fluid circulations

Dissolution and cementation require fluid circulation. The progressive increase in cementation towards the fault planes can be regarded as an indication of fluid migration towards the fault, at least in the first steps of fault formation. A flow outward from the fault, produced by a simple compactive shear band only a few centimetres wide, could not generate such a migration. This view is supported by the increase in permeability (K3) along the fault planes due to the largest pores. Through these pores the migrating fluids could be collected and transferred towards the faults. The contrast in permeability between K3 and K0 and between K3 and K2 illustrates the possibility of concentrated circulations (Table 4, Figs. 10 and 13).

Table 4
Permeabilities obtained from pore modelling based on SEM binary images. K0: intact material. K1: strained material. K2 and K3: faulted material (Fig. 10).

Permeability (mD)	Newhaven (×2000)	Mons I.1 (×350)	Mons I.2 (×2000)	Mons VI.2 (×2000)
K0 (reference)	0.15	0.06	0.25	
K1 (20–30 mm/FP)	0.015	0.02	0.1	
K2 (0–10 mm/FP)	0.01	0.003	0.01	0.01
K3 (large pores)				31.5–36.1

5.3. Fracturing and faulting

The only features observed on the fault planes (Figs. 5b and 11) are compaction, aggregation and coalescence of particles, and formation of smooth striations. A missing 50 mm thick band is the major constraint on the interpretation (Gaviglio et al., 1999; Angelier et al., 2006). One possible process involves the formation of a shear deformation band, either brittle or ductile, concentrating all the deformation by fracturing and dissolution. In view of what is known of the mechanical behaviour of chalk (Schroeder, 2003), both hypotheses have to be considered.

5.4. Dissolution and faulting

Because of the well-ordered orientations of the fault planes, initiation by tectonic shearing is most probable and the dissolution process is only a consequence. However the latter, together with the associated deposition, played such a significant role (Angelier

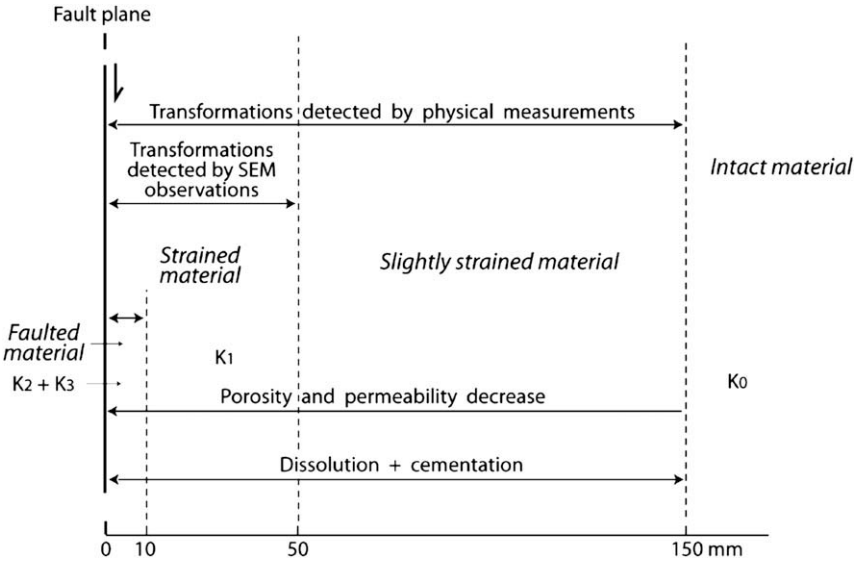

Fig. 10. Organisation of a fault zone based on physical measurements and SEM observations; location of the calculated permeabilities.

et al., 2006) that it is necessary to account for its concentration, either inside a deformation band or upon a single surface. The formation of an initial shear deformation band, either brittle or ductile, brought about the creation of pathways and therefore the possibility of collecting fluids from the unstrained chalk. Based on the present characteristics of the chalk, the circulations between the porous medium and the fault plane (or any fracture mentioned in the following interpretations) are illustrated in Fig. 13.

The characteristics displayed by the chalk can be explained by a ductile shear deformation band. Through disruption of grain contacts, sliding and rotations of grains, the matrix, where voids form large volumes (around 40% in the unstrained chalk), can be reorganised into a more heterogeneous material with some parts looser and others more compact. The formation of looser small volumes can guide the fluids inside the band and therefore initiate a more or less diffuse flow allowing partial drainage of the reservoir. At this stage, dissolution is likely to occur and to be associated with creep; local failures, due to fluid pressure, may cause slip (Fig. 14a). Pervasive dissolution, stimulated by shearing and fluid escape, lead to a narrowing of the shear deformation band, and its progressive closure (Fig. 14b); during that phase, dissolution is the predominant process and it can account for the major part of the downthrow. As a result fluid circulations and displacements tend to be concentrated along a single plane which acts as a shear and dissolution surface (Fig. 14c).

Brittle shear, producing cracks and fractures, might play some part, mainly when deformation is initiated. In that case the shear deformation band becomes a drainage axis (Fig. 14a′) and

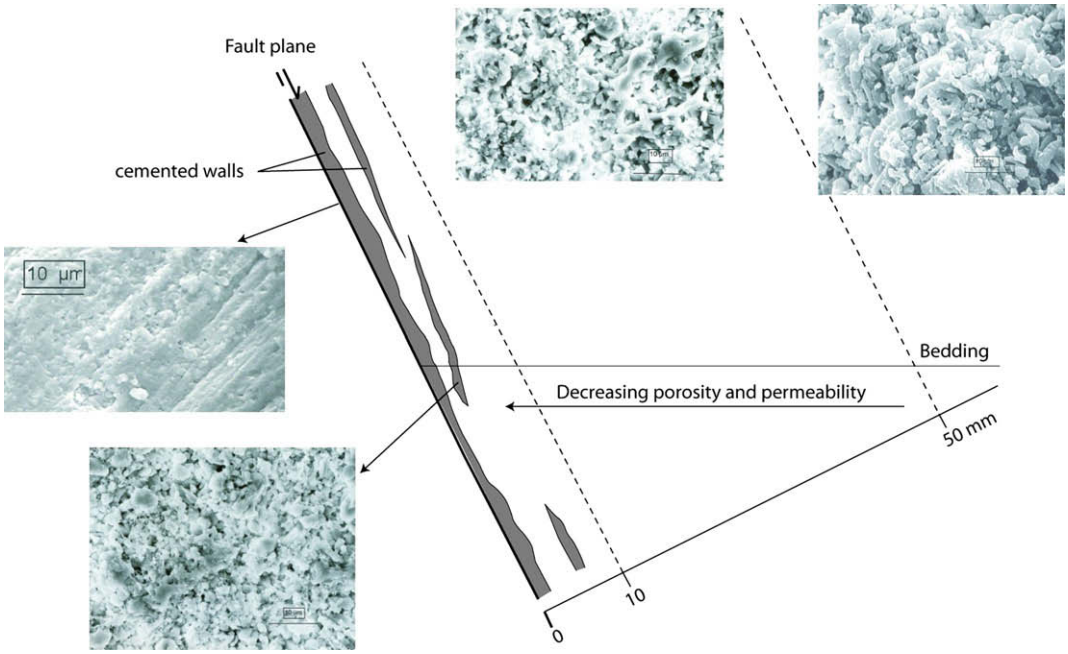

Fig. 11. Distribution of the chalk facies (SEM observations) inside a fault zone.

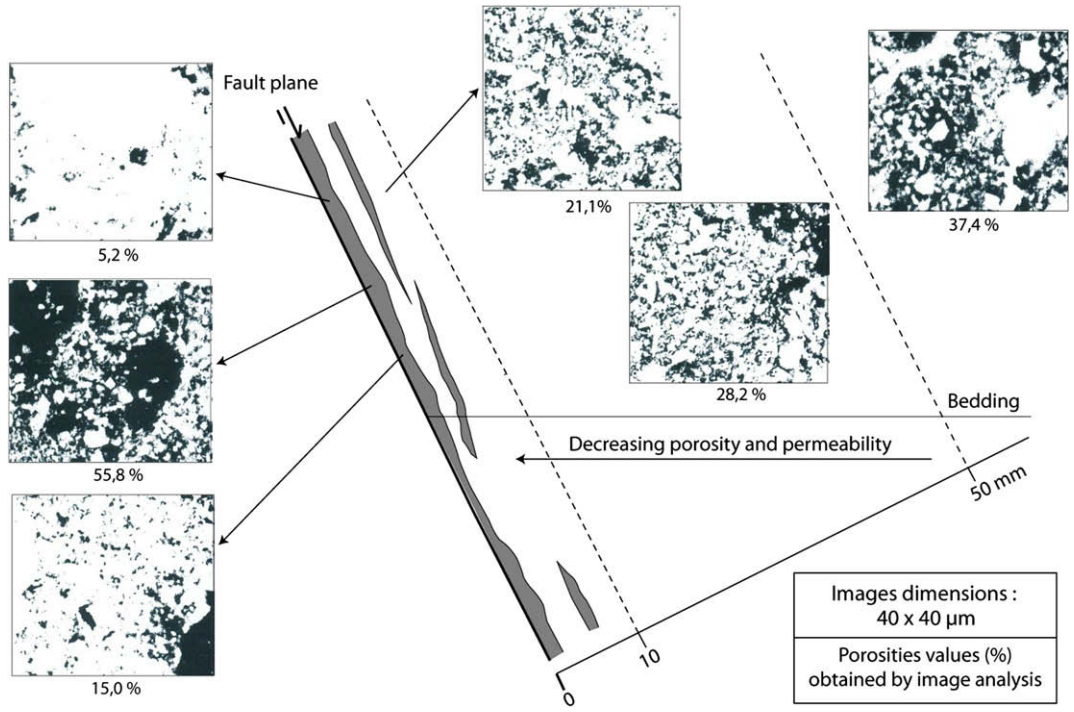

Fig. 12. Binary images illustrating the texture of chalk inside a fault zone. Black areas: voids. The corresponding porosity is given below each image.

dissolution can develop and tend to reduce the width of the band (Fig. 14b′). As a result, the flow, distributed through the whole band, tends to be restricted to a few discontinuities and progressively concentrated along a single one (Fig. 14c). Both dissolution and shearing have a part in producing the downthrow.

Dissolution favoured by tectonic stress conditions can be strongly stimulated when drainage starts because the resulting drop in fluid pressure brings about an increase in effective stresses at the grain contacts; at the same time, deposition of calcite can take place in pores. This process is fundamental whatever shearing, brittle or ductile, occurs. The fault may still be active as long as the tectonic stresses and the permeabilities allow shearing and circulations.

6. Discussion

In the field, no brittle structures can be identified, even as remnants of possible aborted brittle shear deformation bands,

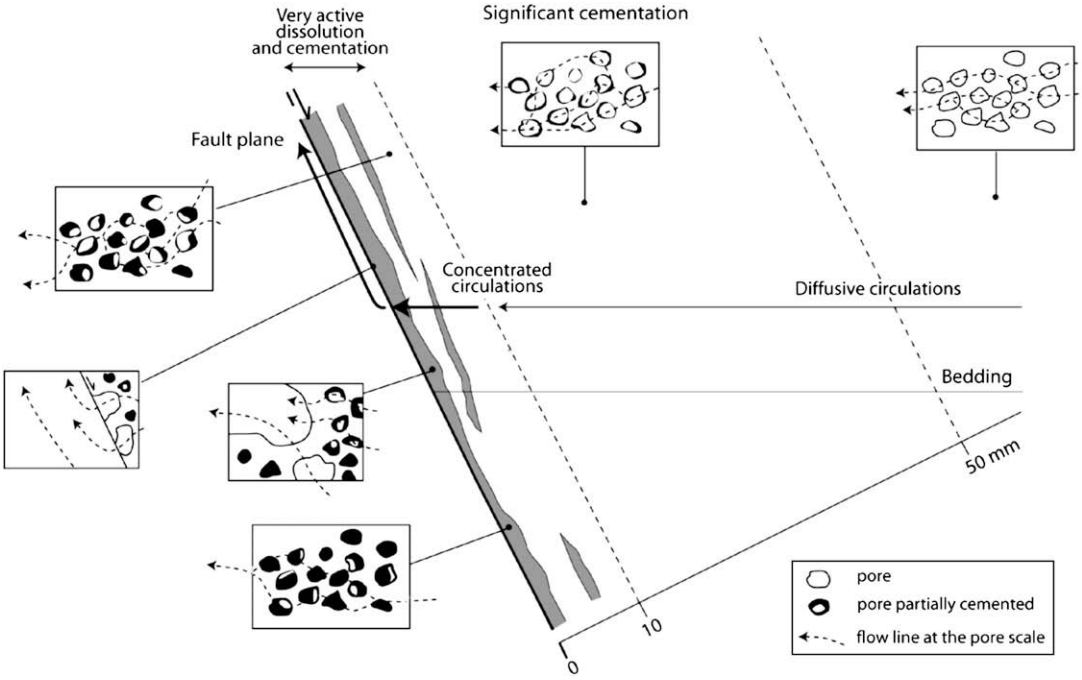

Fig. 13. Interpretation of fluid circulation at the pore level, inside a fault zone.

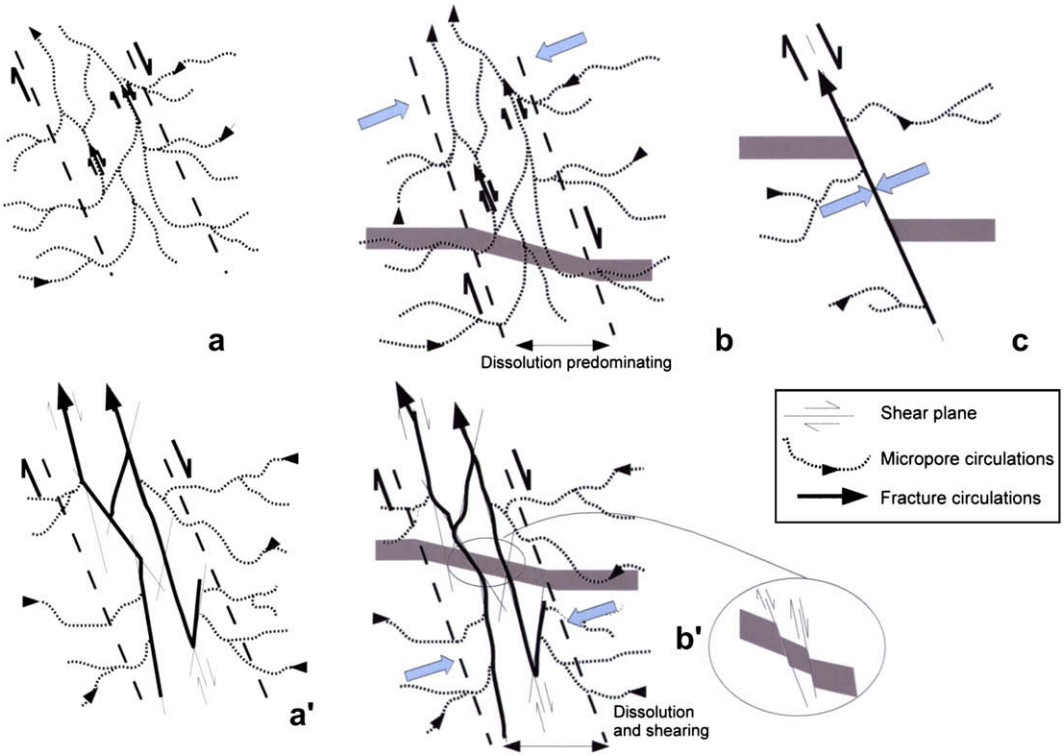

Fig. 14. Possible deformation processes inside a fault zone. See text for detailed explanations. Thick arrows (b, c, b′): shortening due to dissolution.

along the single fault planes. Brittle behaviour cannot be recognized on the grain scale (no evidence of cataclasis, no microcracks); however, it cannot be ruled out because of the very powerful action of dissolution in this medium. If it took place at the beginning of faulting, the structures could be completely obliterated by pressure solution.

We favour an interpretation involving the ductile behaviour. However it is still possible to consider successive ductile and brittle deformation phases; the progressive hardening due to cementation might create conditions for brittle sequences. The microcracks reported in the Newhaven samples might be the consequence of such a hardening. No pore collapse (a common feature in chalk when a high stress level is reached) was detected in this rock. Therefore, in the prevailing stress conditions, due to an overburden less than 500 m, the porosity reduction can be mainly attributed to the fluid circulations. Our interpretation implies that the observed downthrows result from both slip and dissolution creep. Both processes can be closely associated: slip along planes stimulating pressure solution and pressure solution making slip easier.

7. Conclusion

Chalk has a particular mechanical behaviour, hence faulting in chalk cannot be directly compared to that of other common rocks. The textural observations in this study show dissolution and cementation features, associated with a modified organisation of the pore space close to the fault planes. Fluid movements may have taken place towards the fault planes and could be a major factor in chalk deformation. Besides qualitative observations and image analysis, the permeabilities calculated from the properties of the reconstructed media support this view.

Considering the characteristics of the pore system, the fluid circulation and the fault patterns, both the brittle and the ductile shears could be the first stage of faulting. A succession of brittle–ductile phases could also be possible.

Given the predominant dissolution, which probably became more active as deformation progressed, the present state of the fault planes reveals only the last stage when slip and dissolution concentrated on a single surface. This specific behaviour was possible owing to the high porosity of the rock, which favoured slow but massive fluid circulations at the grain level.

Acknowledgements

This study was partially supported by the GDR «Géomécanique des Roches Profondes» and by the French-Belgian Office of Cooperation (Actions intégrées Tournesol). We are grateful to Michèle Adler (CNRS, Meudon) for help during the image analysis work. We thank Marcel Boué for preparing the rock plugs, Serge André (Université de Franche-Comté) and Barbara Ledoux (Faculté Polytechnique de Mons) for drawing the figures. Field observations and sampling were carried out in the Harmignies quarry with the efficient help of Claudio Barcella and Bérénice Deletter (Faculté Polytechnique de Mons). We are grateful to the staff of the "Ciments Belges Réunis" for allowing us to work in very good conditions. This paper benefited from the constructive suggestions of two anonymous reviewers and the editor Thomas Blenkinsop. We are grateful to Nancy Peuteuil who greatly improved the English.

References

Adler, P.M., 1992. Porous Media, Geometry and Transports. Butterworth-Heinemann.
Adler, P.M., Thovert, J.F., 1998. Real porous media: local geometry and macroscopic properties. Applied Mechanics Reviews 51, 537–585.
Adler, P.M., Jacquin, C.G., Quiblier, J.A., 1990. Flow in simulated porous media. International Journal of Multiphase Flow 16 (4), 691–712.

Adler, P.M., Jacquin, C.G., Thovert, J.F., 1992. The formation factor of reconstructed porous media. Water Resources Research 28 (6), 1571–1576.
Angelier, J., Vandycke, S., Bergerat, F., Gaviglio, P., Schroeder, C., Coulon, M., 2006. Can belemnite distribution reveal pressure solution processes along faults? A case study in the chalk of the Mons Basin, Belgium. Journal of Structural Geology 28, 64–82.
Antonellini, M.A., Aydin, A., Pollard, D.D., 1994. Microstructure of deformation bands in porous sandstones at Arches National Park, Utah. Journal of Structural Geology 16, 941–959.
Aydin, A., Borja, R.I., Eichhubl, P., 2006. Geological and mathematical framework for failure modes in granular rocks. Journal of Structural Geology 28, 83–98.
Borre M., Lind I., 1996. Chemical and mechanical processes during burial diagenesis of chalk. An interpretation based on specific surface data of deep sea sediments. In: Proceedings of the Fifth North Sea Chalk Symposium, Reims. Topic VII, 20 pp.
Caine, J.S., Evans, J.P., Forster, C.B., 1996. Fault zone architecture and permeability structure. Geology 24, 1025–1028.
Darquennes, A., Schroeder, C., Vandycke, S., 2006. Petrophysical deformation in faulted white chalk in Belgium. Multiphysics coupling and long term behaviour in rock mechanics. In: Cotthem, Van, Chalier, Thimus, Tshibangu (Eds.), Eurock06-International ISRM Symposium Liège.
Du Bernard, X., Labaume, P., Darcel, C., Davy, P., Bour, O., 2002. Cataclastic slip band distribution in normal fault damage zones, Nubian sandstones, Suez rift. Journal of Geophysical Research 107 ETG 6-1, 6-12.
El Bied, A., Sulem, J., Martineau, F., 2002. Microstructure of shear zones in Fontainebleau sandstone. International Journal of Rock Mechanics and Mining Sciences 39 (7), 917–932.
Gamond, J.F., 1983. Displacement features associated with fault zones: a comparison between observed examples and experimental models. Journal of Structural Geology 5 (1), 33–45.
Gaviglio, P., Adler, P.M., Thovert, J.F., Vandycke, S., Bergerat, F., Bekri, S., Lestideau, R., 1997. Grain-scale microstructures and physical properties of faulted chalk. Bulletin de la Societe Geologique de France 168 (6), 35–47.
Gaviglio, P., Chaye d'Albissin, M., Bergerat, F., Vandycke, S., 1993. Modifications de texture dans la craie au contact de failles normales: un exemple de graben dans le bassin de Mons (Belgique). Bulletin de la Societe Geologique de France 164 (4), 565–575.
Gaviglio, P.M., Vandycke, S., Schroeder, C., Coulon, M., Bergerat, F., Dubois, C., Pointeau, I., 1999. Matrix strains along normal fault planes in the Campanian White Chalk of Belgium: structural consequences. Tectonophysics 309, 41–56.
Hancock, P.L., 1972. The analysis of en échelon veins. Geological Magazine 109 (3), 269–276.
Hancock, P.L., 1985. Brittle microtectonics: principles and practice. Journal of Structural Geology 7 (3/4), 437–457.
Jones, M.E., Leddra, M.J., 1989. Compaction and flow of porous rocks at depth. In: Maury, Fourmaintraux (Eds.), Proc. ISRM-SPE Inter. Symposium Pau, Rock at Great Depth, vol. 2, pp. 891–898.
Matthews A., Sellwood B., Farmer C., 1996. Submarine cementation in chalks of the Valhall and Hod Fields: origin of the «dense zones» as submarine hardgrounds. In: Proceedings of the Fifth North Sea Chalk Symposium, Reims. Topic VII, 19 pp.
Mimran, Y., 1975. Fabric deformation induced in Cretaceous chalks by tectonic stresses. Tectonophysics 26, 309–316.
Mimran, Y., Michaeli, L., 1986. The transition of a major fault into secondary faults in chalk and its effects on the mechanics of the host rock. Israel Journal of Earth Sciences 35, 114–121.
Schroeder C., 2003. Du coccolithe au réservoir pétrolier. Approche phénoménologique du comportement mécanique de la craie en vue de sa modélisation à différentes échelles. Thèse de doctorat, ULG, 169 pp.
Schroeder, C., Gaviglio, P., Bergerat, F., Vandycke, S., Coulon, M., 2006. Faults and matrix deformations in chalk: contribution of porosity and sonic wave velocity measurements. Bulletin de la Societe Geologique de France 177 (4), 203–213.
Segall, P., Pollard, D.D., 1980. Mechanics of discontinuous faults. Journal of Geophysical Research 85 (B8), 4337–4350.
Shipton, Z.K., Cowie, P.A., 2001. Damage zone and slip-surface evolution over μm to km scales in high-porosity Navajo sandstone, Utah. Journal of Structural Geology 23 (12), 1825–1844.
Tchalenko, J.S., 1970. Similarities between shear zones of different magnitudes. Geological Society of America Bulletin 81, 1625–1640.
Thovert, J.F., Salles, J., Adler, P.M., 1993. Computerized characterization of the geometry of real porous media: their discretization, analysis and interpretation. Journal of Microscopy 170, 65–79.
Tondi, E., 2007. Nucleation, development and petrophysical properties of faults in carbonate grainstones: evidences from the San Vito Lo Capo peninsula (Sicily, Italy). Journal of Structural Geology 29, 614–628.
Tondi, E., Antonellini, M., Aydin, A., Marchegiani, L., Cello, G., 2006. The role of deformation bands, stylolites and sheared stylolites in fault development in carbonate grainstones of Majella Mountain, Italy. Journal of Structural Geology 28, 376–391.
Vandycke, S., 1992. Tectonique cassante et paléo-contraintes dans les formations crétacées du nord-ouest européen. Implications géodynamiques. Thèse Univ. Paris VI, Mém. Sc. Terre Univ. Curie, n 92-02, 179 pp.
Vandycke, S., 2002. Paleostress records in Cretaceous formations in NW Europe: extensional and strike-slip events in relationships with Cretaceous–Tertiary inversion tectonics. Tectonophysics 357, 119–136.
Vandycke, S., Bergerat, F., 1989. Analyse microtectonique des déformations cassantes dans le Bassin de Mons. Reconstitution des paléo-champs de contrainte au Crétacé-Tertiaire. Annales Société Géologique de Belgique 112, 479–487.
Vandycke, S., Bergerat, F., Dupuis, C., 1991. Meso-Cenozoic faulting and inferred paleostresses in the Mons Basin, Belgium. Tectonophysics 192, 261–271.